



Optimum Design of FGX-CNT-Reinforced Reddy Pipes Conveying Fluid Subjected to Moving Load

Farid Vakili Tahami¹, Hasan Biglari¹, Morteza Raminnea^{1,*}

¹ Faculty of Mechanical Engineering, University of Tabriz, Tabriz, Iran

Received November 14 2016; revised December 20 2016; accepted for publication December 30 2016.
Corresponding author: Morteza Raminnea, m.raminnea@tabrizu.ac.ir

Abstract

The harmony search algorithm is applied to the optimum designs of functionally graded (FG)-carbon nanotubes (CNTs)-reinforced pipes conveying fluid which are subjected to a moving load. The structure is modeled by the Reddy cylindrical shell theory, and the motion equations are derived by Hamilton's principle. The dynamic displacement of the system is derived based on the differential quadrature method (DQM). Moreover, the length, thickness, diameter, velocity, and acceleration of the load, the temperature and velocity of the fluid, and the volume fraction of CNT are considered for the design variables. The results illustrate that the optimum diameter of the pipe is decreased by increasing the volume percentage of CNTs. In addition, by increasing the moving load velocity and acceleration, the FS is decreased.

Keywords: Pipe, Moving load, Conveying fluid, DQM.

1. Introduction

The optimization of physical systems is a process of variable adjustment which provides an optimum solution for the physical or mechanical problems. By using the random generation of the variables in a part of feasible space and based on the response of the objective problems, the search for the global optimization methods has led to optimum results [1]. In recent years, due to the limitations of the mathematical methods, many researches have been done based on the meta-heuristic algorithms for the optimizations such as genetic algorithms, practical swarm optimization, bees optimization, ant colony optimization, harmony search, firefly algorithms, teaching learning based optimization, cuckoo search algorithm, and etc. One of the newest techniques is the harmony search algorithm (HS) [2]. Geem et al. [2] used the harmony algorithm to solve the mathematical and engineering optimization problems. The successful applications of HS for the optimization problems were provided in Refs. [2-4].

With respect to the developments in the field of pipes under moving load, Hermann and Baker [5] presented an analysis regarding the dynamic response of a long cylindrical sandwich shell under an axially symmetric moving ring load. Huang [6] studied the axially symmetric steady-state response of a linearly elastic, homogeneous, and infinitely long cylindrical shell which was subjected to a ring load traveling at a constant velocity. The dynamic response to a moving ring load of an infinitely long two-layered cylindrical shell was investigated by Chonan [7]. Panneton et al. [8] studied the vibration of a thin cylindrical shell which excited by a constant point load which continuously traveled along the circumferential direction at a rotational speed. Mirzaei et al. [9] reported the analytical and numerical modeling of the transient elasto-dynamic structural response of a cylindrical tube with a finite length to the internal detonation loading. Ruzzene and Bazo [10] used the finite element model (FEM) to analyze the dynamic response of the axisymmetric shells subjected to axially moving loads. Eftekhari [11] used the differential quadrature procedure for the in-plane vibration analysis of the circular arches with variable thickness which were traversed by a moving point load. The thermal effect on the dynamic response of an axially functionally graded beam subjected to a moving harmonic load was presented by Wang and Wu [12].

In this paper, the harmony search algorithm is applied to search the optimum designs of FGX-CNT-reinforced

pipes conveying fluid which are subjected to a moving load based on the Reddy cylindrical shell theory. The length, thickness, diameter, velocity, and acceleration of the load, the temperature and velocity of the fluid, and the volume fraction of CNT are considered for the design variables.

2. Mathematical modeling of the problem

A schematic figure of the FGX-CNT-reinforced pipes conveying fluid which are subjected to a moving load with the length of L , radius of R , and thickness of h is considered.

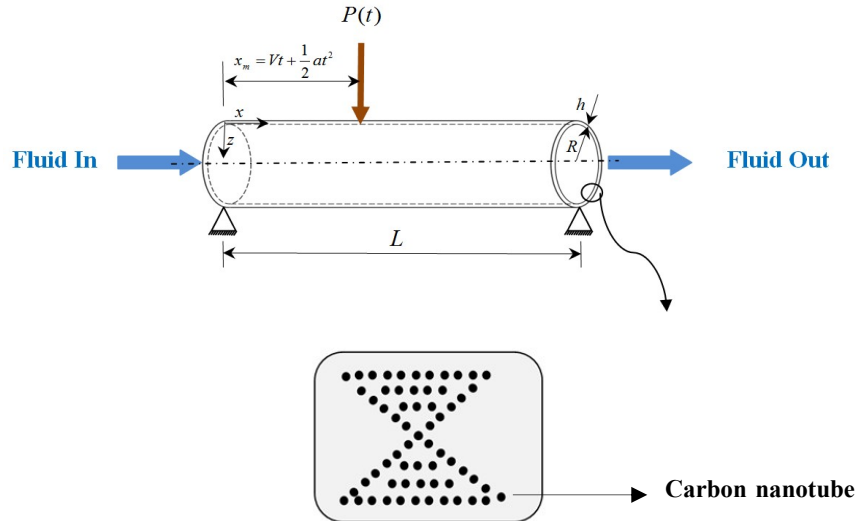


Fig. 1 A schematic figure of the nanocomposite pipe conveying fluid subjected to a moving load

Based on the Reddy shell theory, the displacement field can be expressed as [13]:

$$u_x(x, \theta, z, t) = u(x, \theta, t) + z \psi_x(x, \theta, t) - \frac{4z^3}{3h^2} \left(\psi_x(x, \theta, t) + \frac{\partial}{\partial x} w(x, \theta, t) \right), \tag{1}$$

$$u_\theta(x, \theta, z, t) = v(x, \theta, t) + z \psi_\theta(x, \theta, t) - \frac{4z^3}{3h^2} \left(\psi_\theta(x, \theta, t) + \frac{\partial}{R \partial \theta} w(x, \theta, t) \right), \tag{2}$$

$$u_z(x, \theta, z, t) = w(x, \theta, t), \tag{3}$$

where (u_x, u_θ, u_z) denote the displacement components of an arbitrary point (x, θ, z) in the pipe, and (u, v, w) are the displacement of a material point at (x, θ) on the mid-plane (i.e. $z = 0$) of the pipe along the x -, θ -, and z -directions, respectively; ψ_x and ψ_θ are the rotations of the normal to the mid-plane along the θ - and x -directions, respectively. The von Kármán strains associated with the above displacement field can be expressed in the following form:

$$\begin{Bmatrix} \varepsilon_{xx} \\ \varepsilon_{\theta\theta} \\ \varepsilon_{x\theta} \\ \varepsilon_{xz} \\ \varepsilon_{\theta z} \end{Bmatrix} = \begin{Bmatrix} \varepsilon_{xx}^0 \\ \varepsilon_{\theta\theta}^0 \\ \varepsilon_{x\theta}^0 \\ \varepsilon_{xz}^0 \\ \varepsilon_{\theta z}^0 \end{Bmatrix} + z \begin{Bmatrix} \varepsilon_{xx}^1 \\ \varepsilon_{\theta\theta}^1 \\ \varepsilon_{x\theta}^1 \\ \varepsilon_{xz}^1 \\ \varepsilon_{\theta z}^1 \end{Bmatrix} + z^2 \begin{Bmatrix} \varepsilon_{xx}^2 \\ \varepsilon_{\theta\theta}^2 \\ \varepsilon_{x\theta}^2 \\ \varepsilon_{xz}^2 \\ \varepsilon_{\theta z}^2 \end{Bmatrix} + z^3 \begin{Bmatrix} \varepsilon_{xx}^3 \\ \varepsilon_{\theta\theta}^3 \\ \varepsilon_{x\theta}^3 \\ \varepsilon_{xz}^3 \\ \varepsilon_{\theta z}^3 \end{Bmatrix}, \tag{4}$$

where

$$\begin{Bmatrix} \varepsilon_{xx}^0 \\ \varepsilon_{\theta\theta}^0 \\ \varepsilon_{x\theta}^0 \\ \varepsilon_{xz}^0 \\ \varepsilon_{\theta z}^0 \end{Bmatrix} = \begin{Bmatrix} \frac{\partial u}{\partial x} + \frac{1}{2} \left(\frac{\partial w}{\partial x} \right)^2 \\ \frac{\partial v}{R \partial \theta} + \frac{w}{R} + \frac{1}{2} \left(\frac{\partial w}{R \partial \theta} \right)^2 \\ \frac{\partial v}{\partial x} + \frac{\partial u}{R \partial \theta} + \frac{\partial w}{\partial x} \frac{\partial w}{R \partial \theta} \\ \psi_x + \frac{\partial w}{\partial x} \\ \psi_\theta + \frac{\partial w}{R \partial \theta} \end{Bmatrix}, \tag{5}$$

$$\begin{Bmatrix} \varepsilon_{xx}^1 \\ \varepsilon_{\theta\theta}^1 \\ \varepsilon_{x\theta}^1 \\ \varepsilon_{xz}^1 \\ \varepsilon_{\theta z}^1 \end{Bmatrix} = \begin{Bmatrix} \frac{\partial \psi_x}{\partial x} \\ \frac{\partial \psi_\theta}{R \partial \theta} \\ \frac{\partial \psi_x}{R \partial \theta} + \frac{\partial \psi_\theta}{\partial x} \\ 0 \\ 0 \end{Bmatrix}, \tag{6}$$

$$\begin{Bmatrix} \varepsilon_{xx}^2 \\ \varepsilon_{\theta\theta}^2 \\ \varepsilon_{x\theta}^2 \\ \varepsilon_{xz}^2 \\ \varepsilon_{\theta z}^2 \end{Bmatrix} = \begin{Bmatrix} 0 \\ 0 \\ 0 \\ \frac{-4}{h^2} \left(\psi_x + \frac{\partial w}{\partial x} \right) \\ \frac{-4}{h^2} \left(\psi_\theta + \frac{\partial w}{R \partial \theta} \right) \end{Bmatrix}, \tag{7}$$

$$\begin{Bmatrix} \varepsilon_{xx}^3 \\ \varepsilon_{\theta\theta}^3 \\ \varepsilon_{x\theta}^3 \\ \varepsilon_{xz}^3 \\ \varepsilon_{\theta z}^3 \end{Bmatrix} = \begin{Bmatrix} \frac{-4}{3h^2} \left(\frac{\partial \psi_x}{\partial x} + \frac{\partial^2 w}{\partial x^2} \right) \\ \frac{-4}{3h^2} \left(\frac{\partial \psi_\theta}{R \partial \theta} + \frac{\partial^2 w}{R^2 \partial \theta^2} \right) \\ \frac{-4}{3h^2} \left(\frac{\partial \psi_\theta}{\partial x} + \frac{\partial \psi_x}{R \partial \theta} + 2 \frac{\partial^2 w}{R \partial x \partial \theta} \right) \\ 0 \\ 0 \end{Bmatrix}. \tag{8}$$

The constitutive equation for the stresses σ and the strains ε matrix in the thermal environment may be written as follows:

$$\begin{Bmatrix} \sigma_{xx} \\ \sigma_{\theta\theta} \\ \sigma_{\theta z} \\ \sigma_{zx} \\ \sigma_{x\theta} \end{Bmatrix} = \begin{bmatrix} C_{11}(z,T) & C_{12}(z,T) & 0 & 0 & 0 \\ C_{21}(z,T) & C_{22}(z,T) & 0 & 0 & 0 \\ 0 & 0 & C_{44}(z,T) & 0 & 0 \\ 0 & 0 & 0 & C_{55}(z,T) & 0 \\ 0 & 0 & 0 & 0 & C_{66}(z,T) \end{bmatrix} \begin{Bmatrix} \varepsilon_{xx} - \alpha_{xx} \Delta T \\ \varepsilon_{\theta\theta} - \alpha_{\theta\theta} \Delta T \\ \gamma_{\theta z} \\ \gamma_{zx} \\ \gamma_{x\theta} \end{Bmatrix}, \tag{9}$$

where C_{ij} and $\alpha_{xx}, \alpha_{\theta\theta}$ may be obtained using the Mixture rule [14]. The strain energy can be written as:

$$\begin{aligned} U = & \frac{1}{2} \int_{\Omega_0} \left(N_{xx} \left(\frac{\partial u}{\partial x} + \frac{1}{2} \left(\frac{\partial w}{\partial x} \right)^2 \right) + N_{\theta\theta} \left(\frac{\partial v}{\partial \theta} + \frac{w}{R} + \frac{1}{2} \left(\frac{\partial w}{R \partial \theta} \right)^2 \right) + Q_\theta \left(\frac{\partial w}{R \partial \theta} + \psi_\theta \right) \right. \\ & + Q_x \left(\frac{\partial w}{\partial x} + \psi_x \right) + N_{x\theta} \left(\frac{\partial v}{\partial x} + \frac{\partial u}{R \partial \theta} + \frac{\partial w}{\partial x} \frac{\partial w}{R \partial \theta} \right) + M_{xx} \frac{\partial \psi_x}{\partial x} + M_{\theta\theta} \frac{\partial \psi_\theta}{R \partial \theta} + M_{x\theta} \left(\frac{\partial \psi_x}{R \partial \theta} + \frac{\partial \psi_\theta}{\partial x} \right) \\ & + K_\theta \left(\frac{-4}{h^2} \left(\psi_\theta + \frac{\partial w}{R \partial \theta} \right) \right) + K_x \left(\frac{-4}{h^2} \left(\psi_x + \frac{\partial w}{\partial x} \right) \right) + P_{xx} \left(\frac{-4}{3h^2} \left(\frac{\partial \psi_x}{\partial x} + \frac{\partial^2 w}{\partial x^2} \right) \right) \\ & \left. + P_{\theta\theta} \left(\frac{-4}{3h^2} \left(\frac{\partial \psi_\theta}{R \partial \theta} + \frac{\partial^2 w}{R^2 \partial \theta^2} \right) \right) + P_{x\theta} \left(\frac{\partial \psi_\theta}{\partial x} + \frac{\partial \psi_x}{R \partial \theta} + 2 \frac{\partial^2 w}{R \partial x \partial \theta} \right) \right) dx d\theta, \end{aligned} \tag{10}$$

where the stress resultant-displacement relations can be written as:

$$\begin{Bmatrix} \left\{ \begin{matrix} N_{xx} \\ N_{\theta\theta} \\ N_{x\theta} \end{matrix} \right\}, \left\{ \begin{matrix} M_{xx} \\ M_{\theta\theta} \\ M_{x\theta} \end{matrix} \right\}, \left\{ \begin{matrix} P_{xx} \\ P_{\theta\theta} \\ P_{x\theta} \end{matrix} \right\} \end{Bmatrix} = \int_{-h/2}^{h/2} \begin{Bmatrix} \sigma_{xx} \\ \sigma_{\theta\theta} \\ \sigma_{x\theta} \end{Bmatrix} (1, z, z^3) dz, \tag{11}$$

$$\begin{Bmatrix} \left\{ \begin{matrix} Q_x \\ Q_\theta \end{matrix} \right\}, \left\{ \begin{matrix} K_x \\ K_\theta \end{matrix} \right\} \end{Bmatrix} = \int_{-h/2}^{h/2} \begin{Bmatrix} \sigma_{xz} \\ \sigma_{\theta z} \end{Bmatrix} (1, z^2) dz. \tag{12}$$

The kinetic energy of the system may be written as:

$$K = \frac{\rho}{2} \int_{\Omega_0} \int_{-h/2}^{h/2} \left((\dot{u}_x)^2 + (\dot{u}_\theta)^2 + (\dot{u}_z)^2 \right) dV \quad (13)$$

The external work is divided into two parts: the fluid and moving load; therefore, we have:

$$W = \int_0^L (P_{Fluid} + P_{elastic} + P_{Load}) w dA \quad (14)$$

where the forces are [14, 15]:

$$P_{fluid} = h_f \frac{\partial p_z}{\partial z} = -\rho_f h_f \left(\frac{\partial^2 w}{\partial t^2} + 2Vx \frac{\partial^2 w}{\partial x \partial t} + Vx^2 \frac{\partial^2 w}{\partial x^2} \right) + \mu h_f \left(\frac{\partial^3 w}{\partial x^2 \partial t} + \frac{\partial^3 w}{R^2 \partial \theta^2 \partial t} + Vx \left(\frac{\partial^3 w}{\partial x^3} + \frac{\partial^3 w}{R^2 \partial \theta^2 \partial x} \right) \right) \quad (15)$$

$$P_{load} = F_0 \delta(x - x_m) \quad (16)$$

where μ , Vx , and ρ_f are the viscosity, the mean flow velocity, and the density of the fluid, respectively; F_0 is the amplitude of the moving load; $\delta(x)$ is the Dirac delta-function; and x_m is the position co-ordinate of the moving load in the x -direction which can be defined as:

$$x_m = Vt + \frac{1}{2}at^2 \quad (17)$$

where V and a are the initial velocity and acceleration of the moving load, respectively. Hamilton's principle is:

$$\int (\delta U - \delta K - \delta W) dt = 0 \quad (18)$$

The governing equations can be derived by Hamilton's principle as follows:

$$\begin{aligned} \delta u : & A_{11} \left(\frac{\partial^2 u}{\partial x^2} + \frac{\partial w}{\partial x} \frac{\partial^2 w}{\partial x^2} \right) + A_{12} \left(\frac{\partial^2 v}{R \partial \theta \partial x} + \frac{\partial w}{R \partial x} + \frac{\partial w}{R \partial \theta} \frac{\partial^2 w}{R \partial \theta \partial x} \right) + B_{11} \left(\frac{\partial^2 \psi_x}{\partial x^2} \right) + B_{12} \left(\frac{\partial^2 \psi_\theta}{R \partial \theta \partial x} \right) \\ & + E_{11} \left(\frac{-4}{3h^2} \left(\frac{\partial^2 \psi_x}{\partial x^2} + \frac{\partial^3 w}{\partial x^3} \right) \right) + E_{12} \left(\frac{-4}{3h^2} \left(\frac{\partial^2 \psi_\theta}{R \partial \theta \partial x} + \frac{\partial^3 w}{R^2 \partial x \partial \theta^2} \right) \right) + B_{66} \left(\frac{\partial^2 \psi_x}{R^2 \partial \theta^2} + \frac{\partial^2 \psi_\theta}{R \partial \theta \partial x} \right) \\ & + A_{66} \left(\frac{\partial^2 u}{R^2 \partial \theta^2} + \frac{\partial^2 v}{R \partial \theta^2} + \frac{\partial^2 w}{R \partial \theta \partial x} \frac{\partial w}{R \partial \theta} + \frac{\partial w}{\partial x} \frac{\partial^2 w}{R^2 \partial \theta^2} \right) \\ & + E_{66} \left(\frac{-4}{3h^2} \left(\frac{\partial^2 \psi_\theta}{R \partial \theta \partial x} + \frac{\partial^2 \psi_x}{R^2 \partial \theta^2} + 2 \frac{\partial^3 w}{R^2 \partial x \partial \theta^2} \right) \right) = I_0 \frac{\partial^2 u}{\partial t^2} + J_1 \frac{\partial^2 \psi_x}{\partial t^2} - \frac{4I_3}{h^2} \frac{\partial^3 w}{\partial t^2 \partial x} \end{aligned} \quad (19)$$

$$\begin{aligned} \delta v : & A_{12} \left(\frac{\partial^2 u}{R \partial \theta \partial x} + \frac{\partial w}{\partial x} \frac{\partial^2 w}{R \partial \theta \partial x} \right) + A_{22} \left(\frac{\partial^2 v}{R^2 \partial \theta^2} + \frac{\partial w}{R \partial \theta} + \frac{\partial w}{R \partial \theta} \frac{\partial^2 w}{R^2 \partial \theta^2} \right) + B_{12} \left(\frac{\partial^2 \psi_x}{R \partial \theta \partial x} \right) + B_{22} \left(\frac{\partial^2 \psi_\theta}{R^2 \partial \theta^2} \right) \\ & + E_{12} \left(\frac{-4}{3h^2} \left(\frac{\partial^2 \psi_x}{R \partial \theta \partial x} + \frac{\partial^3 w}{R \partial \theta \partial x^2} \right) \right) + E_{22} \left(\frac{-4}{3h^2} \left(\frac{\partial^2 \psi_\theta}{R^2 \partial \theta^2} + \frac{\partial^3 w}{R^3 \partial \theta^3} \right) \right) + B_{66} \left(\frac{\partial^2 \psi_x}{R \partial \theta \partial x} + \frac{\partial^2 \psi_\theta}{\partial x^2} \right) \\ & + A_{66} \left(\frac{\partial^2 u}{R \partial \theta \partial x} + \frac{\partial^2 v}{\partial x^2} + \frac{\partial^2 w}{\partial x^2} \frac{\partial w}{R \partial \theta} + \frac{\partial w}{\partial x} \frac{\partial^2 w}{R \partial \theta \partial x} \right) + E_{66} \left(\frac{-4}{3h^2} \left(\frac{\partial^2 \psi_\theta}{\partial x^2} + \frac{\partial^2 \psi_x}{R \partial \theta \partial x} + 2 \frac{\partial^3 w}{R \partial x^2 \partial \theta} \right) \right) \\ = & I_0 \frac{\partial^2 v}{\partial t^2} + J_1 \frac{\partial^2 \psi_\theta}{\partial t^2} - \frac{4I_3}{h^2} \frac{\partial^3 w}{R \partial t^2 \partial \theta} \end{aligned}$$

$$\begin{aligned} \delta w : & A_{44} \left(\frac{\partial^2 w}{\partial x^2} + \frac{\partial \psi_x}{\partial x} \right) + D_{44} \left(\frac{-4}{h^2} \left(\frac{\partial \psi_x}{\partial x} + \frac{\partial^2 w}{\partial x^2} \right) \right) + A_{55} \left(\frac{\partial^2 w}{R^2 \partial \theta^2} + \frac{\partial \psi_\theta}{R \partial \theta} \right) + D_{55} \left(\frac{-4}{h^2} \left(\frac{\partial \psi_\theta}{R \partial \theta} + \frac{\partial^2 w}{R^2 \partial \theta^2} \right) \right) \\ & + \frac{\partial}{\partial x} \left(N_{xx} \frac{\partial w}{\partial x} \right) + \frac{\partial}{R \partial \theta} \left(N_{\theta\theta} \frac{\partial w}{R \partial \theta} \right) - \frac{4}{h^2} \left(\left(D_{44} \left(\frac{\partial^2 w}{\partial x^2} + \frac{\partial \psi_x}{\partial x} \right) + F_{44} \left(\frac{-4}{h^2} \left(\frac{\partial^2 w}{\partial x^2} + \frac{\partial \psi_x}{\partial x} \right) \right) \right) \right) \\ & + \left(D_{55} \left(\frac{\partial^2 w}{R^2 \partial \theta^2} + \frac{\partial \psi_\theta}{R \partial \theta} \right) + F_{55} \left(\frac{-4}{h^2} \left(\frac{\partial^2 w}{R^2 \partial \theta^2} + \frac{\partial \psi_\theta}{R \partial \theta} \right) \right) \right) + \frac{4}{3h^2} \left[E_{11} \left(\frac{\partial^3 u}{\partial x^3} + \left(\frac{\partial^2 w}{\partial x^2} \right)^2 \right) + \frac{\partial w}{\partial x} \frac{\partial^3 w}{\partial x^3} \right] \\ & + E_{12} \left(\frac{\partial^3 v}{R \partial \theta \partial x^2} + \frac{\partial^2 w}{R \partial x^2} + \left(\frac{\partial w}{R \partial \theta} \right)^2 + \frac{\partial w}{R \partial \theta} \frac{\partial^3 w}{R \partial x^2 \partial \theta} \right) + F_{11} \left(\frac{\partial^3 \psi_x}{\partial x^3} \right) + F_{12} \left(\frac{\partial^3 \psi_\theta}{R \partial \theta \partial x^2} \right) \\ & + H_{11} \left(\frac{-4}{3h^2} \left(\frac{\partial^3 \psi_x}{\partial x^3} + \frac{\partial^4 w}{\partial x^4} \right) \right) + H_{12} \left(\frac{-4}{3h^2} \left(\frac{\partial^3 \psi_\theta}{R \partial \theta \partial x^2} + \frac{\partial^4 w}{R^2 \partial \theta^2 \partial x^2} \right) \right) + 2E_{66} \left(\frac{\partial^3 u}{R^2 \partial x \partial \theta^2} + \frac{\partial^3 v}{R \partial \theta \partial x^2} \right) \end{aligned} \quad (20)$$

$$\begin{aligned}
& -D_{55} \left(\frac{-4}{h^2} \left(\psi_\theta + \frac{\partial w}{R \partial \theta} \right) \right) + \frac{4}{h^2} \left(D_{55} \left(\frac{\partial w}{R \partial \theta} + \psi_\theta \right) + F_{55} \left(\frac{-4}{h^2} \left(\psi_\theta + \frac{\partial w}{R \partial \theta} \right) \right) \right) \\
& - \frac{4}{3h^2} \left[E_{66} \left(\frac{\partial^2 u}{R \partial \theta \partial x} + \frac{\partial^2 v}{\partial x^2} + \frac{\partial^2 w}{\partial x^2} \frac{\partial w}{R \partial \theta} + \frac{\partial w}{\partial x} \frac{\partial^2 w}{R \partial \theta \partial x} \right) + F_{66} \left(\frac{\partial^2 \psi_x}{R \partial \theta \partial x} + \frac{\partial^2 \psi_\theta}{\partial x^2} \right) \right. \\
& + H_{66} \left(\frac{-4}{3h^2} \left(\frac{\partial^2 \psi_\theta}{\partial x^2} + \frac{\partial^2 \psi_x}{R \partial \theta \partial x} + 2 \frac{\partial^3 w}{R \partial x^2 \partial \theta} \right) \right) + E_{12} \left(\frac{\partial^2 u}{R \partial \theta \partial x} + \frac{\partial w}{\partial x} \frac{\partial^2 w}{R \partial \theta \partial x} \right) \\
& + E_{22} \left(\frac{\partial^2 v}{R^2 \partial \theta^2} + \frac{\partial^2 v}{R^2 \partial \theta} + \frac{\partial w}{R \partial \theta} \frac{\partial^2 w}{R^2 \partial \theta^2} \right) + F_{12} \left(\frac{\partial^2 \psi_x}{R \partial \theta \partial x} \right) + F_{22} \left(\frac{\partial^2 \psi_\theta}{R^2 \partial \theta^2} \right) \\
& + H_{12} \left(\frac{-4}{3h^2} \left(\frac{\partial^2 \psi_x}{R \partial \theta \partial x} + \frac{\partial^3 w}{R \partial \theta \partial x^2} \right) \right) + H_{22} \left(\frac{-4}{3h^2} \left(\frac{\partial^2 \psi_\theta}{R^2 \partial \theta^2} + \frac{\partial^3 w}{R^3 \partial \theta^3} \right) \right) \\
& = J_1 \frac{\partial^2 v}{\partial t^2} + K_2 \frac{\partial^2 \psi_\theta}{\partial t^2} - \frac{4}{3h^2} J_4 \frac{\partial^3 w}{R \partial t^2 \partial \theta}.
\end{aligned} \tag{23}$$

However, using the DQ-IQ methods [14], the motion equations can be written in a compact matrix form as follows:

$$[K_L + K_{NL}][d(t)] + [C][\dot{d}(t)] + [M][\ddot{d}(t)] = [Q(t)], \tag{24}$$

where $[d] = [u \ v \ w \ \psi_x \ \psi_\theta]^T$, $[K_L]$ and $[K_{NL}]$ are the linear and nonlinear stiffness matrixes, respectively, $[C]$ is the damp matrix, and $[M]$ is the mass matrix. Finally, the Newmark- β [16] is applied for calculating the dynamic deflection of the present structure. After that, the stresses of the pipe can be obtained using Eq. (9), and the safety factor can be obtained by the von Mises yield criterion.

3. The harmony search optimization algorithms

Geemet et al. [2] proposed the harmony search (HS) algorithm for optimization problems. HS has been conceptualized from the musical process of searching a perfect state (global optimum) [3]. The harmony quality is enhanced practice after practice, just as the solution quality is enhanced iteration by iteration. The perfect harmony and the improvisation group are corresponding to the global optimum and the design variables, respectively. HS can more accurately search the optimum conditions for an optimization engineering problem with several local minima and discontinuation. The HS algorithm includes five basic steps to search the optimal conditions [2-4]:

- 1) Define the optimization model and the HS parameters
- 2) Determine the initial values of the harmony memory
- 3) Create a new HM
- 4) Update the harmony memory
- 5) Check the stopping criterion: Terminate when the maximum number of improvisation is reached.

The optimization processes of the harmony search algorithm using the above five steps are summarized as follows:

Step 1: Define the optimization problem, the initial values, and the parameters of the algorithm.

The optimization mathematical model for the system is given as follows:

$$\text{find } R, L, h, V_x, V, a_0$$

$$\min \text{ cost} = 100\pi L[(R+h)^2 - R^2](V_s * 56 + (1-V_s) * 460)$$

S t.

$$FS \geq 1;$$

$$R/h \geq 20; R/h \leq 100;$$

$$L/h \geq 1; L/h \leq 100;$$

$$0.015 \leq h \leq 0.03m; 0.5 \leq R \leq 1.5m;$$

$$1 \leq L \leq 6m; 0 \leq V \leq 30m/s; -20 \leq a \leq 20m/s^2;$$

$$0 \leq V_x \leq 500m/s; T = 500; V_s = 0.05 - 0.175,$$

(25)

To search the optimum of the objective function, the sets of design variables are randomly generated based on the parameters of the harmony search which are the harmony memory size (HMS), the harmony memory considering rate (HMCR), the pitch adjusting rate (PAR), the total number of iteration (maximum of improvisation: NI), and the bandwidth (bw). Each generated harmony memory (HM) is randomly improvised using the parameters of HS

including *HMCR*, *PAR*, and *bw* based on three rules: 1) consideration of the previous HM members, 2) adjustment of the existing HM, 3) random selection of each member of HM. *HMCR* shows the selection rate of the new HM elements from the previous HM. *PAR* is similar to the mutation of the GA algorithm and adjusts the decision variables, randomly. Hence, each new design variable is adjusted by bandwidth with the possibility of $PAR \times HMCR$.

Step 2: Define HM with respect to the harmony memory size (HMS) and the random uniform generation from the domain of each variable, which is given as follows:

$$x_i^j = x_i^L + r \times (x_i^U - x_i^L) \tag{26}$$

where $r \in [0,1]$ is a random number. Therefore, each design variable is located on the feasible domain $x_i \in [x_i^L, x_i^U]$. Therefore, the HM matrix is generated as follows:

$$HM = \begin{bmatrix} x_1^1 & x_2^1 & \dots & x_{N-1}^1 & x_N^1 & | & f(x^1) \\ x_1^2 & x_2^2 & \dots & x_{N-1}^2 & x_N^2 & | & f(x^2) \\ \cdot & \cdot & \dots & \cdot & \cdot & | & \cdot \\ x_1^j & x_2^j & \dots & x_{N-1}^j & x_N^j & | & f(x^j) \\ \cdot & \cdot & \dots & \cdot & \cdot & | & \cdot \\ x_1^{HMS-1} & x_2^{HMS-1} & \dots & x_{N-1}^{HMS-1} & x_N^{HMS-1} & | & f(x^{HMS-1}) \\ x_1^{HMS} & x_2^{HMS} & \dots & x_{N-1}^{HMS} & x_N^{HMS} & | & f(x^{HMS}) \end{bmatrix} \tag{27}$$

In the present paper, the bandwidth for the design variables are considered based on the lower and upper bounds of each design variable as:

$$bw_i = (x_i^U - x_i^L) / 1000 \tag{28}$$

Step 3: Improve a new HM based on the parameters of the HS algorithm.

The memory consideration, pitch adjustment, and randomization are applied to improve the new HM for each design variable in the standard HS algorithm as follows:

IF $r_1 \leq HMCR$ **then**

$$x_i'^j = x_i^j ; \tag{29} \quad / \text{Selecting from the previous harmony memory}/$$

IF $r_2 \leq PAR$ **then**

$$x_i'^j = x_i^j + (2r - 1) \times bw_i ; \tag{30} \quad / \text{Adjusting the new harmony memory}/$$

ENDIF

ELSE

$$x_i'^j = x_i^L + r_3 \times (x_i^U - x_i^L) ; \tag{31} \quad / \text{Selecting from the domain of variables}/$$

ENDIF;

$$F'^j = f(x'^j) ; \tag{32} \quad / \text{Computing the cost function based on the new harmony memory}/$$

where, x' is the new HM, r, r_1, r_2, r_3 are the random numbers which are selected in the range from 0-1. The new HM with probability of *HMCR* is selected from the old HM. Then, the new memory is adjusted with the probability of $PAR \times HMCR$ using the uniform distribution and the bandwidth in Eq. (25). The *PAR* and *bw* are considered as constant values for all the iterations of HS.

Step 4: Update HM based on the new objective function ($f(x'^j)$) if $f(x'^j)$ has much better optimum than the previous objective function ($f(x^j)$), then HM is updated by the new memory and the worst decision vector is deleted from HM.

Step 5: Continue the steps 3 and 4 to achieve a good solution or the maximum number of iteration.

4. Results and discussion

In this research, the pipe is made of the Poly methyl methacrylate (PMMA) with the constant Poisson's ratio of $\nu_m = 0.34$, the temperature-dependent thermal coefficient of $\alpha_m = (1 + 0.0005\Delta T) \times 10^{-6} / K$, and the temperature-dependent Young moduli of $E_m = (3.52 - 0.0034T) GPa$ in which $T = T_0 + \Delta T$ and $T_0 = 300 K$ (room temperature). In addition, (10, 10) CNTs are selected as reinforcements with the material properties reported in Ref. [14]. The application of HS for optimization of the structure is presented in this section. All codes are written in MATLAB 7.0 and run on Intel (R) Core (TM) i5 Laptop with two 2.53 GHz CPU processors and 4.0 GB RAM memory. The constraint optimization model in Eq. (25) is computed by the penalty method based on an

unconstrained cost function (CF) as follows:

$$CF = Cost + \lambda[g(FS)]^\eta \tag{29}$$

in which λ and η are the penalty coefficients as $\lambda = 10^8$ and $\eta = 2$. $g(FS)$ is the penalty function which is computed as follows:

$$g(FS) = \min\{0, FS - 1\} \tag{30}$$

where the $Cost$ is the cost to provide the material and FS is the safety factor of the nanocomposite pipe which can be computed based on the mathematical modeling in Eq. (25).

The parameters of the HS algorithm for optimization of the structure are considered as HMS=10, NI=10000, HMCR=0.95, and PAR= 0.35 [2-4]. The optimization designs for the nanocomposite pipe are obtained based on the $V_s=0.1$, as $R^*=1.40893$ m, $h^*=0.015$ m, $L^*=1$ m, $V^*=5$ m/s, $a^*=-20$ m/s², and $V_x^*=500$ m/s. It can be concluded that the variables V (velocity of the moving load), a (acceleration of the moving load), h (the thickness of the pipe), and L (the length of the pipe) are converged to lower their bounds, and V_x (the velocity of the fluid) is tended to the upper bounds to achieve optimum conditions. The variable R is selected as the optimum design factor of this example.

As shown in Fig. 2(a)-(c), the cost function, the optimum radius, and FS of the structure are plotted versus the volume percentage of CNTs (V_s) in the pipe for different moving load accelerations, respectively. It can be seen that by increasing the volume percent of CNTs, the cost and optimum radius of the pipe decreases, while the FS is improved. It is due to the fact that by increasing the volume percentage of CNTs, the stiffness of the structure increases; however, the optimum radius decreases, and FS increases. The decrease of the cost by an increase in the volume percentage of CNTs is due to the higher cost of PMMA compared with CNTs. However, by increasing the volume percentage of CNTs, the volume percentage of PMMA decreases, hence, the cost of the structure reduces. In addition, by increasing the moving load accelerations, the optimum radius of the pipe increases; as a result, the cost increases. In other words, increasing the moving load accelerations leads to a decrease in the safety of the pipes as a result of a decrease in FS. It is also found that after $V_s=0.1$, the effect of the moving load accelerations on FS becomes ignorable.

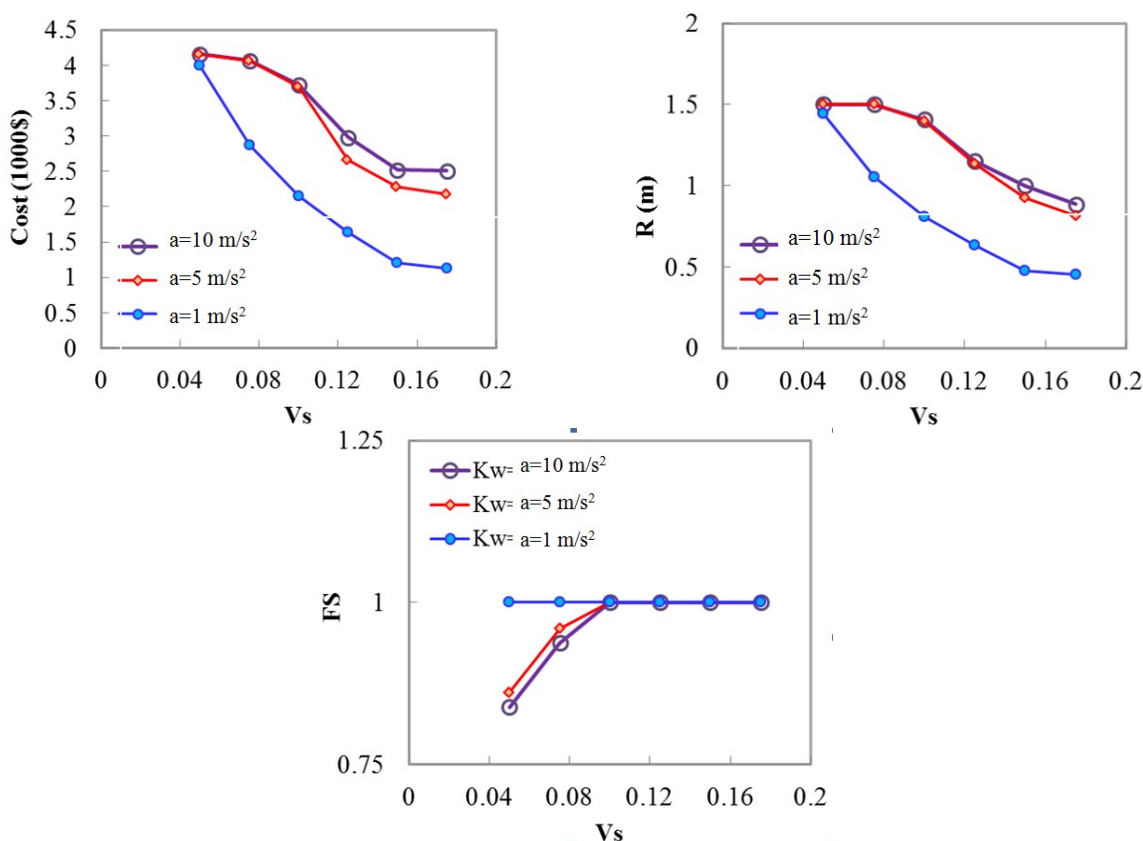


Fig. 2 The effect of the moving load acceleration on the (a) cost versus volume percentage of CNTs (b) optimum radius versus volume percentage of CNTs (c) FS versus volume percentage of CNTs

Fig. 3(a)-(c) presents the cost, the optimum radius, and FS versus the volume percentage of CNTs for different moving load velocity, respectively. It is obvious that the cost and optimum radius of the structure are decreased by increasing the volume percentage of CNTs, while FS is increased. As an important result, by increasing the moving load velocity, the cost and optimum radius of the pipe are enhanced, while FS is decreased. This is physically logical, since increasing the moving load velocity leads to a decrease in the stability of the pipe. However, the safety factor of the pipe decreases, and since the optimum radius of the pipe is increased, the cost of the pipe increases.

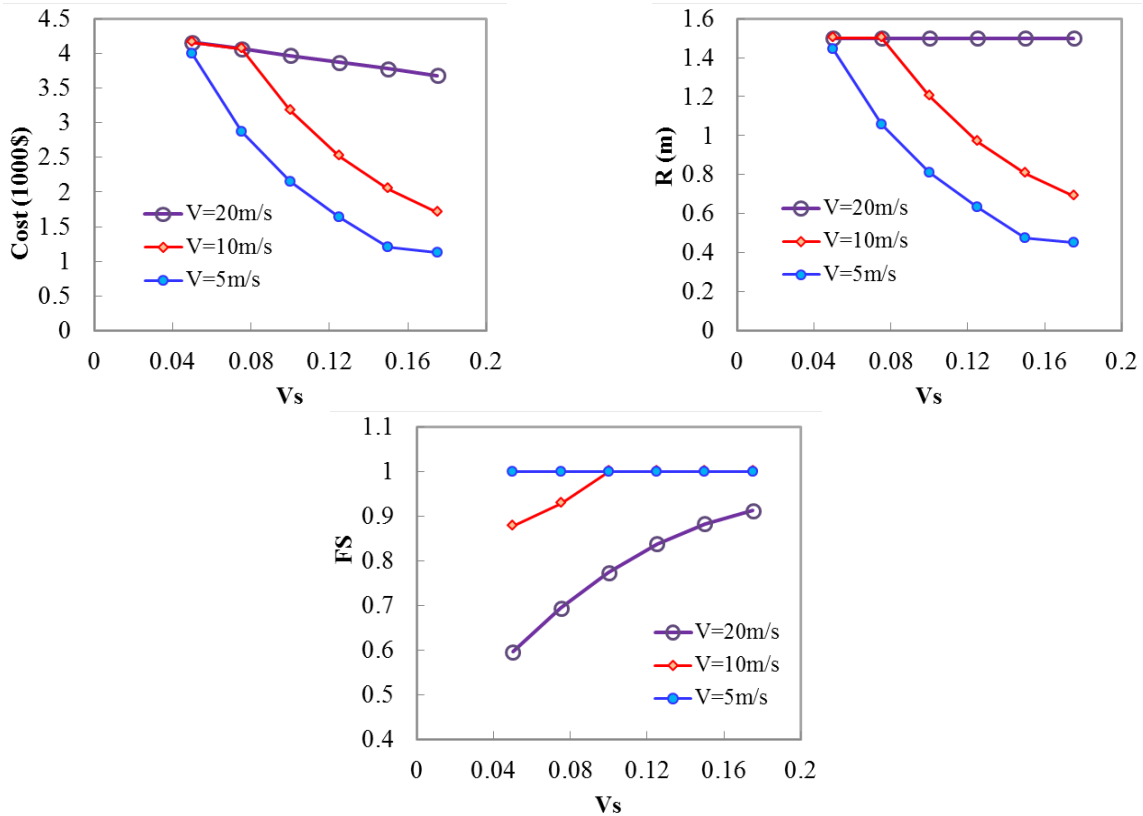


Fig. 3 The effect of the moving load velocity on the (a) cost versus volume percentage of CNTs (b) optimum radius versus volume percentage of CNTs (c) FS versus volume percentage of CNTs

The effects of the thickness of the pipe on the cost, the optimum radius, and FS are illustrated in Fig. 3(a)-(c) with respect to the volume percentage of CNTs, respectively. As shown in Fig. 4, increasing the volume percentage of CNTs leads to a decrease in the cost and optimum radius of the structure. It is also concluded that by increasing the thickness of the pipe, the cost increases, while the optimum radius of the pipe decreases, since the stiffness of the structure enhances. It is also worth mentioning that the thickness of the pipe in the range between 0.015 to 0.02 m, does not have any considerable effect on FS.

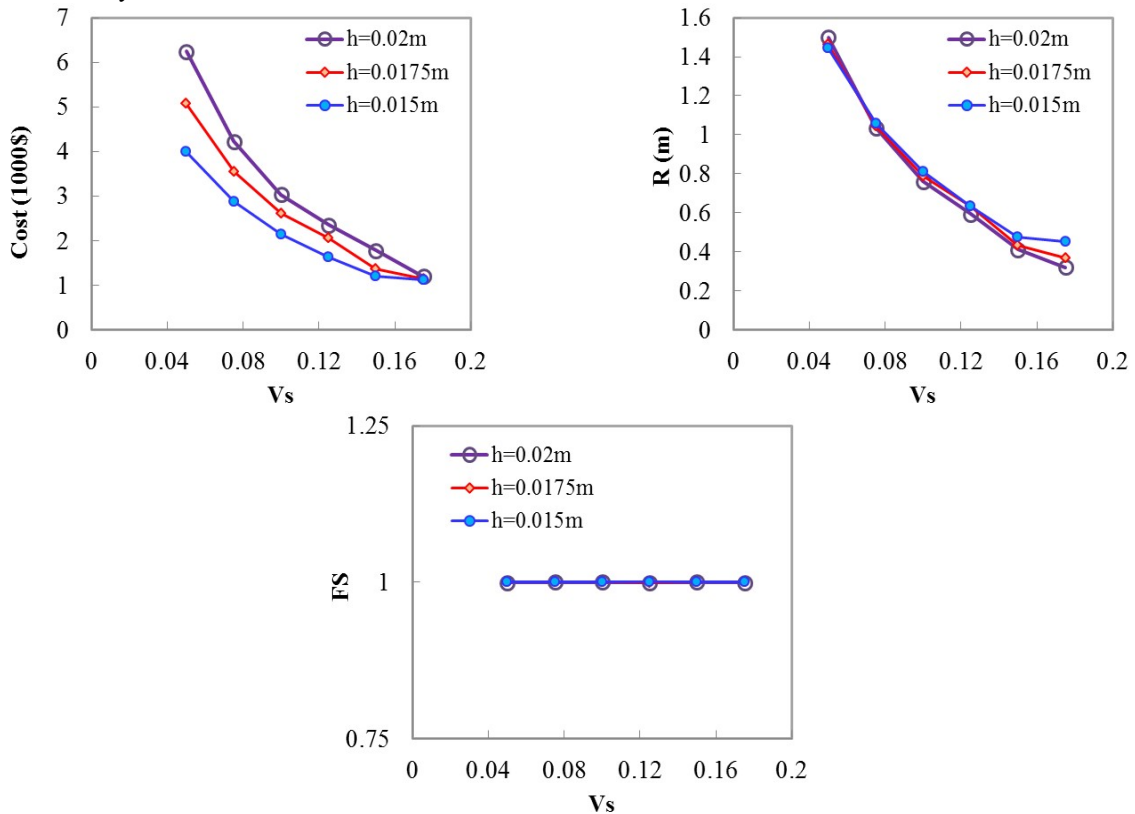


Fig. 4 The effect of the thickness of the pipe on the (a) cost versus volume percentage of CNTs (b) optimum radius versus volume percentage of CNTs (c) FS versus volume percentage of CNTs

percentage of CNTs (c) FS versus volume percentage of CNTs

The effects of the fluid velocity on the cost function, the optimum radius, and FS are illustrated in Fig. 5(a)-(c) as a function of the volume percentage of CNTs, respectively. As can be seen, by increasing the fluid velocity, FS is decreased as well. This is considered reasonable, since increasing the fluid velocity leads to instability in the pipe. It is also found that the cost and optimum radius are increased by increasing the fluid velocity. Furthermore, the cost and optimum radius of the pipe are decreased by increasing the CNTs volume percentage, while the safety factor increases.

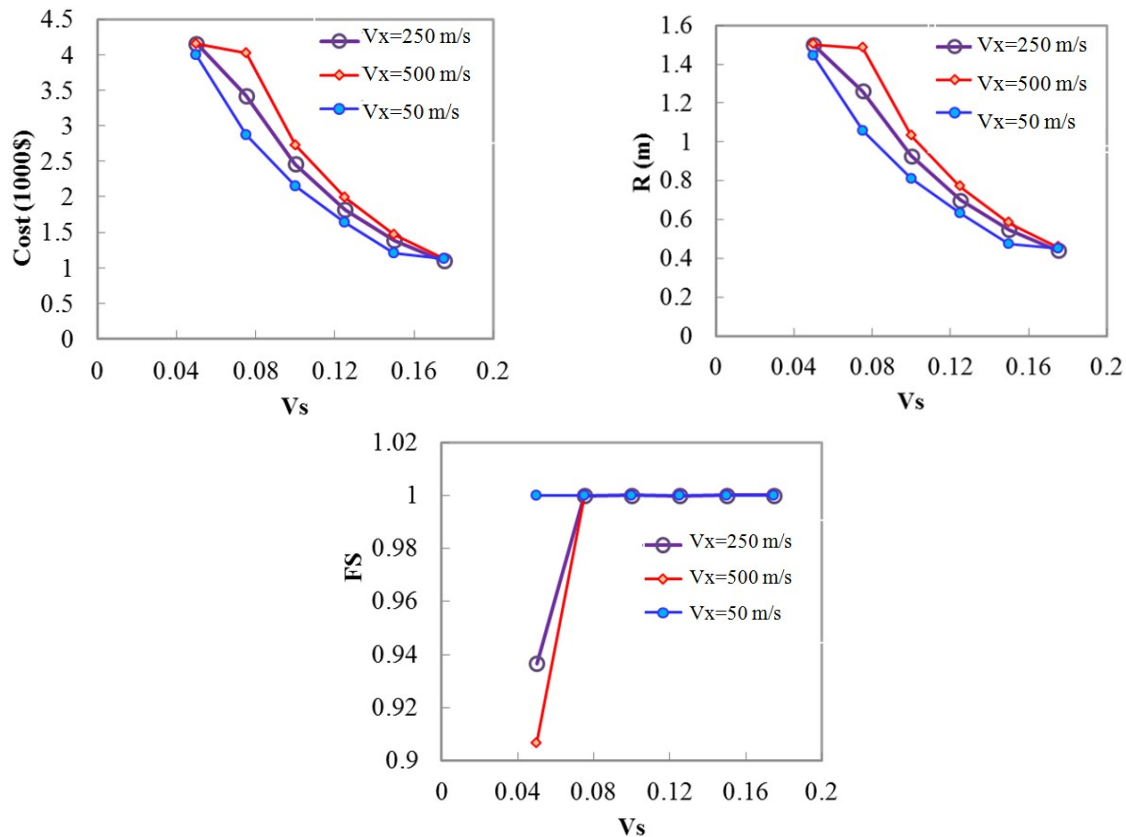


Fig. 5 The effect of the fluid velocity on the (a) cost versus volume percentage of CNTs (b) optimum radius versus volume percentage of CNTs (c) FS versus volume percentage of CNTs

References

- [1] Keshtegar, B. and Oukati Sadeq, M., "Gaussian global-best harmony search algorithm for optimization problems", *Soft Computing*, 2016, doi:10.1007/s00500-00016-02274-z.
- [2] Geem, Z.W., Kim, J.H. and Loganathan, G., "A new heuristic optimization algorithm: harmony search", *Simulation*, Vol. 76, pp. 60-68, 2001.
- [3] Lee, K.S. and Geem, Z.W., "A new meta-heuristic algorithm for continuous engineering optimization: harmony search theory and practice", *Computer methods in applied mechanics and engineering*, Vol. 194, pp. 3902-3933, 2005.
- [4] Omran, M.G. and Mahdavi, M., "Global-best harmony search", *Applied mathematics and computation*, Vol. 198, pp. 643-656, 2008.
- [5] Hermann, G. and Baker, E.H., "Response of cylindrical sandwich shells to moving loads", *Transaction ASME Journal of Applied Mechanics*, Vol. 34, pp. 1-8, 1967.
- [6] Huang, C.C., "Moving loads on elastic cylindrical shells", *Journal of Sound and Vibrations*, Vol. 49, pp. 215-20, 1976.
- [7] Chonan, S., "Moving load on a two-layered cylindrical shell with imperfect bonding", *The Journal of the Acoustical Society of America*, Vol. 69, pp. 1015-20, 1981.
- [8] Panneton, R., Berry, A. and Laville F., "Vibration and sound radiation of a cylindrical shell under a circumferentially moving load", *The Journal of the Acoustical Society of America*, Vol. 98, pp. 2165-73, 1995.
- [9] Mirzaei, M., Biglari, H. and Slavatiyan, M., "Analytical and numerical modeling of the transient elasto-dynamic response of a cylindrical tube to internal gaseous detonation", *International Journal of Pressure Vessels and Piping*, Vol. 83, pp. 531-539, 2006.
- [10] Ruzzene, M. and Baz, A., "Dynamic stability of periodic shells with moving loads. *Journal of Sound and Vibrations*, Vol. 296, pp. 830-44, 2006.
- [11] Eftekhari, S.A., "Differential quadrature procedure for in-plane vibration analysis of variable thickness circular

- arches traversed by a moving point load”, *Applied Mathematical Modelling*, Vol. 40, pp. 4640-4663, 2016.
- [12] Wang, Y. and Wu, D., “Thermal effect on the dynamic response of axially functionally graded beam subjected to a moving harmonic load”, *Acta Astronautica*, Vol. 127, pp. 17-181, 2016.
- [13] Reddy, J.N., “A Simple Higher Order Theory for Laminated Composite Plates”, *Journal of Applied Mechanics*, Vol. 51, pp. 745–752, 1984.
- [14] Kolahchi, R., Safari, M. and Esmailpour, M., “Dynamic stability analysis of temperature-dependent functionally graded CNT-reinforced visco-plates resting on orthotropic elastomeric medium”, *Composite Structures*, Vol. 150, pp. 255-265, 2016.
- [15] Raminnea, M., Biglari, H. and Vakili Tahami, F., “Nonlinear higher order Reddy theory for temperaturedependent vibration and instability of embedded functionally graded pipes conveying fluid-nanoparticle mixture”, *Structural Engineering and Mechanics*, Vol. 59, pp. 153-186, 2016.
- [16] Simsek, M. and Kocaturk, T., “Nonlinear dynamic analysis of an eccentrically prestressed damped beam under a concentrated moving harmonic load”, *Journal of Sound and Vibration*, Vol. 320, pp. 235–253, 2009.